Fiber-Based Cylindrical Vector Beams and Its Applications to Optical Manipulation

Renxian Li, Lixin Guo, Bing Wei, Chunying Ding and Zhensen Wu

Additional information is available at the end of the chapter

1. Introduction

Radiation pressure force (RPF) indeced by a focused laser beam has bean widely utlized for the manipulation of small particles, and has found more and more applications in various fields including physics [1], biology [2], and optofludics [3, 4]. Accurate prediction of optical force exerted on particles enables better understanding of the physical mechanicsm, and is of great help for the design and improvement of optical tweezers.

Many researches have been devoted to the prediction of radiation pressure force (RPF), and different approaches have been developed for the theoretical calculation of RPF exerted on a homogeneous sphere. The geometrical optics [5-7] and Rayleigh theory [8] are respectively considered for the particles much larger and smaller than the wavelength of incident beam. Since geometrical optics and Rayleigh theory are both approximation theories, rigorous theories based on Maxwell's theory have been considered [9-13]. Generalized Lorenz-Mie Theory (GLMT) [14] has been used to investigate the RPFs exerted on some regular parti-cles[10-13, 15, 16] induced by a Gaussian beam. GLMT can rigorously calculate RPF induced by any beam. To isolate the contribution of various scattering process to RPF, Debye series is introduced [17, 18].

Traditional optical tweezers use Gaussian beams as trapping light sources. This approach works well for the manipulation of microscopic spheres. However, the deveopment of science and technology brings new challenges to optical tweezers, and several approaches have been developed. Holographic methods have been used to increase the strength and dexterity of optical trap [19]. Another approch is the employment of non-Gaussian beam including Laguerre-Gaussian beams [20] and Bessel beams [28]. Laguerre-Gaussian beams have zero on-

axis intensity, and can increase the strength of optical trap. Bessel beams consist of a series of concentric rings of decreasing intensity, and have characteristics of non-diffraction and self-reconstruction. A single Bessel beam can be used to simultaneously trap and manipulate, accelerate, rotate, or guide many particles. Bessel beams can trap and manipulate both high-index and low-index particles.

In addition to Laguerre-Gaussian and Bessel beams, there is a speical class of beams which have cylindrical symmetry in both amplitude and polarization, hence the name Cylindrical Vector Beams (CVBs) [29-32]. CVBs are solutions of vector wave equation in the paraxial limit. The special features of CVBs have attracted considerable interest for a variety of novel applications, including lithography, particle acceleration, material processing, high-resolution metrology, atom guiding, optical trapping and manipulation. The most interesting features for optical trapping arise from the focusing properties of CVBs. A radially polarized beam focused by a high numerical aperture objective has a peak at the focus, and can trap a high-index particle. On the contrary, an azimuthally polarized beam has null central intensity, and can trap low-index particle. These two kinds of beams can be experimentally switched.

CVBs can be generated by many methods, which are categorized as active or passive depending on whether amplifying media is used. The simplest mothod is to convert an incident Gaussian beam to a radially polarized beam using a radial polariser. However this method does not produce very high purity tansverse modes. Moer efficient methods use interferometry. Since a CVB can be expressed as the linear superpostion of two Hermite-Gaussian or Laguerre-Gaussian beams with different orientations of polarization. Another efficient method is based on optical fiber [33]. This technique takes advantage of the similarity between the poarization propeties of the modes that propagate inside a step-index optical fiber and CVBs. When TE_{01} or TM_{01} is excited in the fibre, it excites a CVB in free space. Fiber-generated CVB, taking Bessel-Gaussian as example, and its applicaions top optical manipulations will be discussed in this chapter.

2. Mathematical description of cylindrical vector beams

Cylindrical vector beams are solutions of vector wave equation

$$\nabla \times \nabla \times \vec{E} + k^2 \vec{E} = 0, \tag{1}$$

where $k=2\pi/\lambda$ is wavenumber with λ being the wavelength. In the paraxial approximation, the radially and azimuthally polarized vector Bessel-Gaussian beams, two kinds of typical CVBs, can be expressed as

$$\vec{E}_{rad} = E_0 \frac{\rho}{w_0} e^{-\frac{\rho^2}{w_0^2}} e^{i(\omega t - kz)} \hat{e}_\rho \tag{2}$$

$$\vec{E}_{azi} = E_0 \frac{\rho}{w_0} e^{-\frac{\rho^2}{w_0^2}} e^{i(\omega t - kz)} \hat{e}_\phi \tag{3}$$

where r and ϕ are respectively the radial and azimuthal coordinates, $\hat{e}_\rho$ and $\hat{e}_\phi$ are unit vectors in ρ and ϕ directions, and the subscripts *rad* and *azi* denote the polarization state. w_0 is the width of beam waist, and E_0 is a constant. Fig. 1(a) and (b) respectively give the intensity distribution of radially and azimuthally polarized Bessel-Gaussian beam in the plane *z=0*. Note that the longitudial component of CVB is negligible under the condition of paraxial approximation. A general CVB can be considered as a linear superposition of a radially polarized CVB and an azimuthally polarized one.
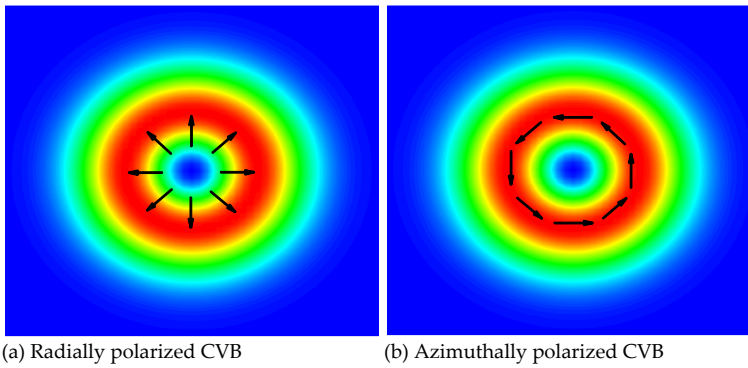

(a) Radially polarized CVB   (b) Azimuthally polarized CVB

Figure 1. Intensity distribution of CVB. The arrows indicate the direction of polarization

3. Radiation force induced by CVB

3.1. Optical force on Rayleigh particles

In the Rayleigh regime, particles can be considered as infinitesimal induced dipoles which interact with incident beam. Here we assume that the particle is a microsphere. RPF will be decomposed into scattering force and gradient force.

The oscillating dipole, which is induced by time-harmonic fields, can be considered as an antenna. The antenna will radiate energy. The difference between energy removed from incident beam and energy radiated by the antenna accounts for the change of momentum flux, and hence rusults in a scattering force. The scattering force can be expressed as

$$\vec{F}_{scat} = \hat{e}_z C_{pr} n_1^2 \varepsilon_0 |E|^2 \tag{4}$$

with

$$C_{pr} = C_{scat} = \frac{8}{3}\pi(ka)^4 a^2 \left(\frac{m^2-1}{m^2+2}\right)^2 \tag{5}$$

and

$$m = n_2 / n_1 \tag{6}$$

where n_1 is the refractive index of surrounding media, and n_2 is the refractive index of the particle. a is the radius of microsphere. ε_0 is the dielectric constant in the vacumm. Note that the scattering force always points in the direction of incident beam.

When a particle is illuminated by a non-uniform electric field, it will experience a gradient force.

$$\vec{F}_{grad} = \pi n_1^2 \varepsilon_0 a^3 \left(\frac{m^2-1}{m^2+2}\right) \nabla |E|^2 \tag{7}$$

For a time-harmonic field, the gradient force can also be expressed in terms of the intensity I of incident beam:

$$\vec{F}_{grad} = \frac{2\pi n_1 a^3}{c} \left(\frac{m^2-1}{m^2+2}\right) \nabla I \tag{8}$$

where c is the speed of light in the vacumm. It is obvious that the gradient force depends on the gradient of the intensity. By sbustituting Eqs. (2) and (3) into Eqs. (4) and (7), we can obtain the scattering and gradient force of vector Bessel-Gaussian beams exerted on a microsphere. For radially polarized Bessel-Gaussian beam, they can be expressed as

$$\vec{F}_{scat} = \hat{e}_z C_{pr} n_1^2 \varepsilon_0 E_0^2 \frac{\rho^2}{w_0^2} \left(e^{-\frac{\rho^2}{w_0^2}} \right)^2 \tag{9}$$

$$\vec{F}_{grad} = \pi n_1^2 \varepsilon_0 a^3 \left(\frac{m^2-1}{m^2+2}\right) \left[\frac{2E_0^2\rho}{w_0^2} \left(e^{-\frac{\rho^2}{w_0^2}} \right)^2 - \frac{4E_0^2\rho^3}{w_0^4} \left(e^{-\frac{\rho^2}{w_0^2}} \right)^2 \right] \hat{e}_\rho \tag{10}$$

From Eq. (10), we can find that the gradient force has only ϱ component. This is because $|E|^2$ is only dependent on ϱ. Here we give only the force for radially polarized beam incidence, and that for azimuthally polarized beam incidence can be derived in the same way.

3.2. Radiation force exerted on Mie particles

Many practical particles manipulated with optical tweezers, such as bioloical cells, are Mie particles, whose size is in the order of the wavelength of trapping beam. To calculate the radiation force exerted on such particles, a rigorous electromagnetic theory based on the Maxwell equations must be considered. Generalized Lorenz-Mie Thoery (GLMT) developed by Gouesbet et al. can solve the interaction between homogeneous spheres and focused beams with any shape, and has been entended to solve the scattering of shaped beam by multilayered spheres, homogeneous and multilayered cylinders, and homogeneous and multilayered spheroids. GLMT has been applied to the rigorous calculation of radiation pressure and optical torque. In GLMT, the incident beam is described by a set of beam shape coefficients(BSCs), which can be evaluated by integral localized approximation (ILA) [34].

This section is devoted to the GLMT for radiation force exerted on a sphere illuminated by a vetor Bessel-Gaussian beam. The general theory for radiation force based on electromagnetic scattering theory is followed by BSCs for CVB. To clarify the physical interpretation of various features of RPF that are implicit in the GLMT, Debye Series Expansion (DSE) is introduced.

3.2.1. Generizination Lorenz-Mie theory

Consider a sphere with radius a and refractive index m_1 illuminated by a CVB of wavelength λ in the surrounding media. The center of the sphere is located at O_P, origin of the Cartesian coordinate system $O_{P\text{-}xyz}$. The beam center is at O_G, origin of coordinate system $O_{G\text{-}uvw}$, with u axis parallel to x and similarly for the others. The coordinates of O_G in the system $O_{P\text{-}xyz}$ is (x_0, y_0, z_0). The refractive index of surrounding media is m_2. The other parameters are defined in Fig. 2.

When a sphere is illuminated by focused beam, the RPF is proportional to the net momentum removed from the incident beam, and can be expressed in terms of the surface integration of Maxwell stress tensor

$$< \mathbf{F} > = < \oint_S \mathbf{n} \cdot \vec{\widehat{T}} dS >$$ (11)

where $< >$ represents a time average, $\overset{\wedge}{\boldsymbol{n}}$ the outward normal unit vector, and S a surface enclosing the particle. The Maxwell stress tensor $\vec{T}$ is given by

$$< \vec{T} > = \frac{1}{4\pi} \left(\varepsilon \mathbf{EE} + \mathbf{HH} - \frac{1}{2} \left(\varepsilon E^2 + H^2 \right) \vec{I} \right)$$ (12)
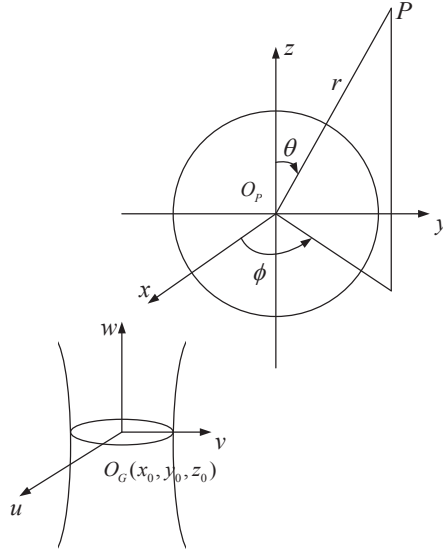
Figure 2. Coordinate systems in GLMT. $O_{P\text{-}xyz}$ is attached to the sphere, and $O_{G\text{-}uvw}$ to the incident beam.

Where the electromagnetic fields E and H are the total fields, namely the sum of the incident and scattered fields, given by

$$\mathbf{E} = \mathbf{E}_i + \mathbf{E}_s, \mathbf{H} = \mathbf{H}_i + \mathbf{H}_s \tag{13}$$

E_i and H_i are the incident electromagnetic wave, and can be expanded as:

$$E_r^i = \frac{E_0}{k_0^2 r^2} \sum_{n=1}^{\infty} \sum_{m=-n}^{+n} c_n^{pw} g_{n,TM}^m n(n+1) \psi_n(k_0 r) P_n^{|m|}(\cos\theta) e^{(im\varphi)} \tag{14}$$

$$E_\theta^i = \frac{E_0}{k_0 r} \sum_{n=1}^{\infty} \sum_{m=-n}^{+n} c_n^{pw} \left[g_{n,TM}^m \psi_n'(k_0 r) \tau_n^{|m|}(\cos\theta) + m g_{n,TE}^m \psi_n(k_0 r) \pi_n^{|m|}(\cos\theta) \right] e^{(im\varphi)} \tag{15}$$

$$E_\varphi^i = i \frac{E_0}{k_0 r} \sum_{n=1}^{\infty} \sum_{m=-n}^{+n} c_n^{pw} \left[m g_{n,TM}^m \psi_n'(k_0 r) \pi_n^{|m|}(\cos\theta) + g_{n,TE}^m \psi_n(k_0 r) \tau_n^{|m|}(\cos\theta) \right] e^{(im\varphi)} \tag{16}$$

$$H_r^i = \frac{H_0}{k_0^2 r^2} \sum_{n=1}^{\infty} \sum_{m=-n}^{+n} c_n^{pw} g_{n,TE}^m n(n+1) \psi_n(k_0 r) P_n^{|m|}(\cos\theta) e^{(im\varphi)} \tag{17}$$

$$H_\theta^i = -\frac{H_0}{k_0 r} \sum_{n=1}^{\infty} \sum_{m=-n}^{+n} c_n^{pw} \left[m g_{n,TM}^m \psi_n(k_0 r) \pi_n^{|m|}(\cos\theta) - g_{n,TE}^m \psi_n'(k_0 r) \tau_n^{|m|}(\cos\theta) \right] e^{(im\varphi)} \tag{18}$$

$$H_\varphi^i = -\frac{iH_0}{k_0 r} \sum_{n=1}^{\infty} \sum_{m=-n}^{+n} c_n^{pw} \left[g_{n,TM}^m \psi_n(k_0 r) \tau_n^{|m|}(\cos\theta) - m g_{n,TE}^m \psi_n'(k_0 r) \pi_n^{|m|}(\cos\theta) \right] e^{(im\varphi)} \tag{19}$$

with

$$\pi_n^m(\cos\theta) = \frac{dP_n^m(\cos\theta)}{d\theta} \tag{20}$$

$$\tau_n^m(\cos\theta) = m \frac{P_n^m(\cos\theta)}{\sin\theta} \tag{21}$$

$$c_n^{pw} = (-i)^{n+1} \frac{2n+1}{n(n+1)} \tag{22}$$

where $P_n^m(\cos\theta)$ represents the associated Legendre polynomials of degree n and order m, $\psi(\cdot)$ is the spherical Ricatti-Bessel functions of first kind, and the prime indicates the derivative of the function with respect to its argument. $g_{n,TM}^m$ and $g_{n,TE}^m$ are so-called BSCs and will be discussed in next subsection.

Similarly, the scattered fields E_s and H_s have the expression :

$$E_r^s = -\frac{E_0}{k_0^2 r^2} \sum_{n=1}^{\infty} \sum_{m=-n}^{+n} c_n^{pw} A_n^m n(n+1) \xi_n(k_0 r) P_n^{|m|}(\cos\theta) e^{(im\varphi)} \tag{23}$$

$$E_\theta^s = -\frac{E_0}{k_0 r} \sum_{n=1}^{\infty} \sum_{m=-n}^{+n} c_n^{pw} \left[A_n^m \xi_n'(k_0 r) \tau_n^{|m|}(\cos\theta) + m B_n^m \xi_n(k_0 r) \pi_n^{|m|}(\cos\theta) \right] e^{(im\varphi)} \tag{24}$$

$$E_\varphi^s = -i \frac{E_0}{k_0 r} \sum_{n=1}^{\infty} \sum_{m=-n}^{+n} c_n^{pw} \left[m A_n^m \xi_n'(k_0 r) \pi_n^{|m|}(\cos\theta) + B_n^m \xi_n(k_0 r) \tau_n^{|m|}(\cos\theta) \right] e^{(im\varphi)} \tag{25}$$

$$H_r^s = -\frac{H_0}{k_0^2 r^2} \sum_{n=1}^{\infty} \sum_{m=-n}^{+n} c_n^{pw} B_n^m n(n+1) \xi_n(k_0 r) P_n^{|m|}(\cos\theta) e^{(im\varphi)} \tag{26}$$

$$H_\theta^s = \frac{H_0}{k_0 r} \sum_{n=1}^{\infty} \sum_{m=-n}^{+n} c_n^{pw} \left[m A_n^m \xi_n(k_0 r) \pi_n^{|m|}(\cos\theta) - B_n^m \xi_n'(k_0 r) \tau_n^{|m|}(\cos\theta) \right] e^{(im\varphi)} \tag{27}$$

$$H_\varphi^s = \frac{iH_0}{k_0 r} \sum_{n=1}^{\infty} \sum_{m=-n}^{+n} c_n^{pw} \left[A_n^m \xi_n(k_0 r) \tau_n^{|m|}(\cos\theta) - m B_n^m \xi_{nn}^{'}(k_0 r) \pi_n^{|m|}(\cos\theta) \right] e^{(im\varphi)} \tag{28}$$

Where $\xi_n(k_0 r)$ is Ricatti-Hankel functions, and scattering coefficients A_n^m and B_n^m can be expressed by traditional Mie scattering coefficients a_n, b_n and BSCs $g_{n,TM}^m$, $g_{n,TE}^m$:

$$A_n^m = a_n g_{n,TM}^m, \qquad B_n^m = b_n g_{n,TE}^m \tag{29}$$

with

$$a_n = \frac{-m_1 \psi_n^{'}(x)\psi_n(y) + m_2 \psi(x)\psi_n^{'}(y)}{-m_1 \xi_n^{(1)'}(x)\psi_n(y) + m_2 \xi_n^{(1)}(x)\psi_n^{'}(y)} \tag{30}$$

$$b_n = \frac{-m_2 \psi_n^{'}(x)\psi_n(y) + m_1 \psi(x)\psi_n^{'}(y)}{-m_2 \xi_n^{(1)'}(x)\psi_n(y) + m_1 \xi_n^{(1)}(x)\psi_n^{'}(y)} \tag{31}$$

$$x = m_2 k_0 a, \qquad y = m_1 k_0 a \tag{32}$$

Substituting Eqs. (14) - (19) and (23) - (28) into Eqs. (11) - (12), and after some algebra, we can get the formula for RPFs which can be characterized by radiation pressure cross section (RPCS):

$$\mathbf{F}(\mathbf{r}) = \frac{2_2 I_0}{c} \left[\hat{\mathbf{e}}_\mathbf{x} C_{pr,x}(\mathbf{r}) + \hat{\mathbf{e}}_\mathbf{y} C_{pr,y}(\mathbf{r}) + \hat{\mathbf{e}}_\mathbf{z} C_{pr,z}(\mathbf{r}) \right] \tag{33}$$

where RPCS $C_{pr,i}$ ($i = x, y, z$) has a longitudinal cross section $C_{pr,z}$

$$\begin{aligned}
C_{pr,z} = \frac{\lambda^2}{\pi} \sum_{n=1}^{\infty} Re \Bigg\{ & \frac{1}{n+1} (A_n g_{n,TM}^0 g_{n+1,TM}^{0*} + B_n g_{n,TE}^0 g_{n+1,TE}^{0*}) + \sum_{m=1}^{n} \Bigg[\frac{1}{(n+1)^2} \frac{(n+m+1)!}{(n-m)!} \\
& \times (A_n g_{n,TM}^m g_{n+1,TM}^{m*} + A_n g_{n,TM}^{-m} g_{n+1,TM}^{-m*} + B_n g_{n,TE}^m g_{n+1,TE}^{m*} + B_n g_{n,TE}^{-m} g_{n+1,TE}^{-m*}) \\
& + m \frac{2n+1}{n^2(n+1)^2} \frac{(n+m)!}{(n-m)!} C_n (g_{n,TM}^m g_{n,TE}^{m*} - g_{n,TM}^{-m} g_{n,TE}^{-m*}) \Bigg] \Bigg\}
\end{aligned} \tag{34}$$

and two transverse cross section $C_{pr,x}$ and $C_{pr,y}$

$$C_{pr,x} = \text{Re}(C) \qquad C_{pr,y} = \text{Im}(C) \tag{35}$$

where

$$C = \frac{\lambda^2}{2\pi} \sum_{n=1}^{\infty} \left\{ -\frac{(2n+2)!}{(n+1)^2} F_n^{n+1} + \sum_{m=1}^{n} \frac{(n+m)!}{(n-m)!} \frac{1}{(n+1)^2} \right.$$
$$\times \left[F_n^{m+1} - \frac{n+m+1}{n-m+1} F_n^m + \frac{2n+1}{n^2} (C_n g_{n,TM}^{m-1} g_{n,TE}^{m*} \right.$$
$$\left. \left. - C_n g_{n,TM}^{-m} g_{n+1,TE}^{-m+1*} + C_n^* g_{n,TE}^{m-1} g_{n,TM}^{m*} - C_n^* g_{n,TE}^{-m} g_{n,TM}^{-m+1*}) \right] \right\} \tag{36}$$

with

$$F_n^m = A_n g_{n,TM}^{m-1} g_{n+1,TM}^{m*} + B_n g_{n,TE}^{m-1} g_{n+1,TE}^{m*} + A_n^{m*} g_{n+1,TM}^{-m} g_{n,TM}^{-m+1*} + B_n^{m*} g_{n+1,TE}^{-m} g_{n,TE}^{-m+1*} \tag{37}$$

$$A_n = a_n + a_{n+1}^* - 2a_n a_{n+1}^* \tag{38}$$

$$B_n = b_n + b_{n+1}^* - 2b_n b_{n+1}^* \tag{39}$$

$$C_n = -i(a_n + b_{n+1}^* - 2a_n b_{n+1}^*) \tag{40}$$

Note that substituting Eq. (13) into Eqs. (11) - (12) shows that the total RPF can be devided into thress parts:

$$< \mathbf{F} > = < \mathbf{F}_i > + < \mathbf{F}_{mix} > + < \mathbf{F}_s > \tag{41}$$

where $<F_i>$ depends only on the incident fields, $<F_s>$ is associated with the scattered fields, and $<F_{mix}>$ involves the interactions of the incident beam with the scattered field. After a great deal of algebra, we can get that $<F_i>=0$, which can be understood by the momentum conservation law for monochromatic fields in free space. The RPCS for $<F_{mix}>$ and $<F_s>$ can be directly given using Eqs. (34) - (40) by changing Eqs. (38) - (40) using

$$A_n = a_n + a_{n+1}^*$$
$$B_n = b_n + b_{n+1}^* \tag{42}$$
$$C_n = -i(a_n + b_{n+1}^*)$$

for $<F_{mix}>$, and

$$A_n = -2a_n a_{n+1}^*$$
$$B_n = -2b_n b_{n+1}^* \tag{43}$$
$$C_n = 2ia_n b_{n+1}^*$$

for $<F_s>$.

3.2.2. Beam shape coefficients for CVB

This section is devoted the derivation of BSCs for CVB using ILA. In the ILA, the beam shape coefficients $g_{n,TM}^m$ and $g_{n,TE}^m$ are obtained respectively from the radial component of electric and magnetic field E_r and H_r according to [34]

$$g_{n,TE}^m = \frac{Z_n^m}{2\pi H_{B0}} \int_0^{2\pi} \overline{H}_r(r,\theta,\phi)\mathrm{e}^{-im\phi}d\phi \tag{44}$$

$$g_{n,TM}^m = \frac{Z_n^m}{2\pi E_{B0}} \int_0^{2\pi} \overline{E}_r(r,\theta,\phi)\mathrm{e}^{-im\phi}d\phi \tag{45}$$

with

$$Z_n^m = \begin{cases} \dfrac{2n(n+1)i}{2n+1} & m=0 \\[2mm] \left(\dfrac{-2i}{2n+1}\right)^{|m|-1} & m \neq 0 \end{cases} \tag{46}$$

$\overline{E}_r$ and $\overline{H}_r$ are respectively the localized fields of E_r and H_r, and they are obtained by changing kr to $(n+1/2)$ and θ to $\pi/2$ in their expression. For a radially polarized Bessel-Gaussian beam, the localized radial component of electric field are derived from Eq. (2):

$$\begin{aligned} \overline{E}_{rad}^r &= E_0\overline{\Omega}_0 \left[-(\rho_n\cos\phi - \xi_0)\cos\phi + (\rho_n\sin\phi - \eta_0)\sin\phi \right] \\ &= E_0\overline{\Omega}_0 \left[\rho_n - \rho_0\sin(\phi+\phi_0) \right] \end{aligned} \tag{47}$$

with

$$\overline{\Omega}_0 = -\sqrt{2}\exp\left[-(\rho_n^2 + \xi_0^2 + \eta_0^2)\right]\exp\left[2\rho_n(\xi_0\cos\phi + \eta_0\sin\phi)\right] \tag{48}$$

$$\rho_n = \frac{kr}{kw_0} = \frac{1}{kw_0}\left(n+\frac{1}{2}\right) \tag{49}$$

$$\xi_0 = \rho_0\sin\phi_0, \quad \eta_0 = \rho_0\cos\phi_0 \tag{50}$$

Substituting Eq. (47) into Eq. (45), and considering the formula of Bessel function

$$J_n(x) = \frac{1}{2\pi}\int_{-\pi}^{\pi} e^{i(x\sin\theta - n\theta)}d\theta = \frac{1}{2\pi}\int_{0}^{2\pi} e^{i(x\sin\theta - n\theta)}d\theta \tag{51}$$

we can obtain the final expression of BSCs

$$g_{n,TM}^{m,rad} = \frac{1}{2}Z_n^m\overline{\Omega}_n e^{im\phi_0}\left[2\rho_n J_m(-2i\rho_n\rho_0) + i\rho_0\left(J_{m-1}(-2i\rho_n\rho_0) - J_{m+1}(-2i\rho_n\rho_0)\right)\right] \tag{52}$$

Here we only derive $g_{n,TM}^{m,rad}$, and $g_{n,TE}^{m,rad}$ can be derived in the similar way.

3.2.3. Debye series expansion

GLMT is a rigorous electromagnetic theory, and can exactly predict the RPF exerted on a sphere by focused beam. Whereas the solution is complicated combinations of Bessel functions, and the mathematical complexity obscures the physical interpretation of various features of RPF. The DSE, which is a rigorous electromagnetic theory, expresses the Mie scattering coefficients into a series of Fresnel coefficients and gives physical interpretation of different scattering processes. The DSE is an efficient technique to make explicit the physical interpretation of various features of RPF which are implicit in the GLMT. The DSE is firstly presented by Debye in 1908 for the interaction between electromagnetic waves and cylinders. Since then, the DSE for electromagnetic scattering by homogeneous, coated, multilayered spheres, multilayered cylinders at normal incidence, homogeneous, multilayered cylinder at oblique incidence, and spherical gratings are studied. In our previous work, DSE has been employed to the analysis of RPF exerted on a sphere induced by a Gaussian and Bessel beam.

As shown in Fig. 3, when an incoming spherical multipole wave, which is

$$\Psi = \xi_n^{(1)}(m_2 kr)P_n^m(\cos\theta)\begin{Bmatrix}\cos m\phi \\ \sin m\phi\end{Bmatrix}, \tag{53}$$

encounters the interface of the sphere at $r=a$, portion of it will be transmitted into the sphere, and another portion will reflected back. The transmitted and reflected waves are respectively:

$$\Psi_1 = T_n^{21}\xi_n^{(1)}(m_1 kr)P_n^m(\cos\theta)\begin{Bmatrix}\cos m\phi \\ \sin m\phi\end{Bmatrix} \qquad r \le a \tag{54}$$

$$\Psi_2 = \left[\xi_n^{(1)}(m_2 kr) + R_n^{212}\xi_n^{(2)}(m_2 kr)\right]P_n^m(\cos\theta)\begin{Bmatrix}\cos m\phi \\ \sin m\phi\end{Bmatrix} \qquad r \ge a \tag{55}$$
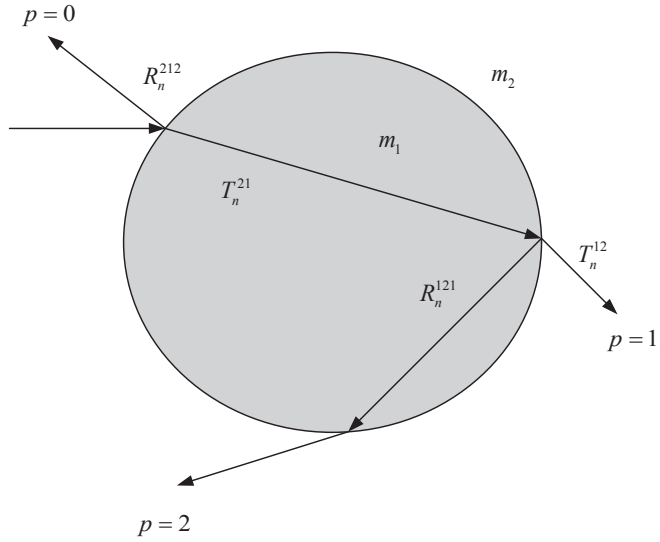
Figure 3. Debye model of light scattering by a sphere

Applying the boundary conditions, which reqires continuity of the tangential components of filds at the interface, to the incident, transmitted and reflected waves,we can obtain:

$$T_n^{21} = \frac{m_1}{m_2} \frac{2i}{D_n} \tag{56}$$

$$R_n^{212} = \frac{\alpha \xi_n^{(1)'}(\kappa_2) \xi_n^{(1)}(\kappa_1) - \beta \xi_n^{(1)}(\kappa_2) \xi_n^{(1)'}(\kappa_1)}{D_n} \tag{57}$$

with

$$D_n = -\alpha \xi_n^{(2)'}(\kappa_2) \xi_n^{(1)}(\kappa_1) + \beta \xi_n^{(2)}(\kappa_2) \xi_n^{(1)'}(\kappa_1) \tag{58}$$

$$\kappa_j = m_j ka \tag{59}$$

$$\alpha = \begin{cases} 1, & for\ TE \\ \dfrac{m_1}{m_2}, & for\ TM \end{cases}, \qquad \beta = \begin{cases} \dfrac{m_1}{m_2}, & for\ TE \\ 1, & for\ TM \end{cases} \tag{60}$$

Similarly, the consideration of outgoing multipole waves can get

$$T_n^{12} = \frac{2i}{D_n} \tag{61}$$

$$R_n^{121} = \frac{\alpha \xi_n^{(2)'}(\kappa_2) \xi_n^{(2)}(\kappa_1) - \beta \xi_n^{(2)}(\kappa_2) \xi_n^{(2)'}(\kappa_1)}{D_n} \tag{62}$$

Substituting all Fresnel coefficients into

$$\left(1 - R_n^{121}\right)\left(1 - R_n^{212}\right) - T_n^{21} T_n^{12} \tag{63}$$

and after much algebra, we get

$$\begin{aligned}
\left.\begin{array}{c} a_n \\ b_n \end{array}\right\} &= \frac{1}{2}\left[1 - R_n^{212} - \frac{T_n^{21} T_n^{12}}{1 - R_n^{121}}\right] \\
&= \frac{1}{2}\left[1 - R_n^{212} - \sum_{p=1}^{\infty} T_n^{21}\left(R_n^{121}\right)^{p-1} T_n^{12}\right]
\end{aligned} \tag{64}$$

where the prime indicates the derivative of the function with respect to its argument. $\xi_n^{(1)}(\cdot)$ and $\xi_n^{(2)}(\cdot)$ are respectively the spherical Ricatti-Hankel functions of first and second kinds. The definition of all Fresnel coefficients and Debye term p are given in Fig. 3. For convenience, we note p = - 1 and p = 0 respectively for the diffraction and direct reflection. In our previous work, we have theoretically and numerically proved that when p ranges from 1 to , the Eq. (64) is identical to the traditional Mie scattering coefficients. Here we provide the DSE for homogeneous spheres, and the DSE for multilayered spheres can be found in our previous work.

4. Numerical results and discussions

In this section, the GLMT and DSE will be employed to analyze the RPF exerted on a homogeneous sphere induced by a radially polarized vector Bessel-Gaussian beam. Xu et al. used GLMT to analyze the RPF exerted on a slightly volatile silocone oil of refractive index , which can be levitated in the air by a beam of wavelength . We first use GLMT to analyze the RPF exerted on such oil induced by vector Bessel-Gaussian beam, and DSE will be employed to the study of the contribution of various scattering process to RPF. In our calculation, the radius of the particle is .

We first explore the influence of beam center location on the RPF. In our calculation, we assume the beam center is located on the x axis so that . Fig. 4 gives the transverse RPCS ∞ versus m_1=1.5 for various beam-waist radius λ =0.5μm. Here we consider a=2.5μm and y_0=z_0=0, which are respectively larger, equal and smaller than the radius of the particle. We can find that the particle can not be trapped at the beam center $C_{pr,x}$ for all beams. This results from the fact all beams have null central intensity. It is worth pointing out that a stable trap corresponds to a particle position where the RPF is zero and its slope is positive. All curves have two equilibrium points, which are symmetric with respect to beam axis (x_0). This is decided by the intensity maxima of beams. So a vector Bessel-Gaussian beam can simultaneously trap more than one particles. We can also find that the interval of equilibrium points increases with the increasing of w_0. This can be easily explained from the fact that the interval of intensity peaks increases with the increasing of w_0=5μm, 2.5μm.
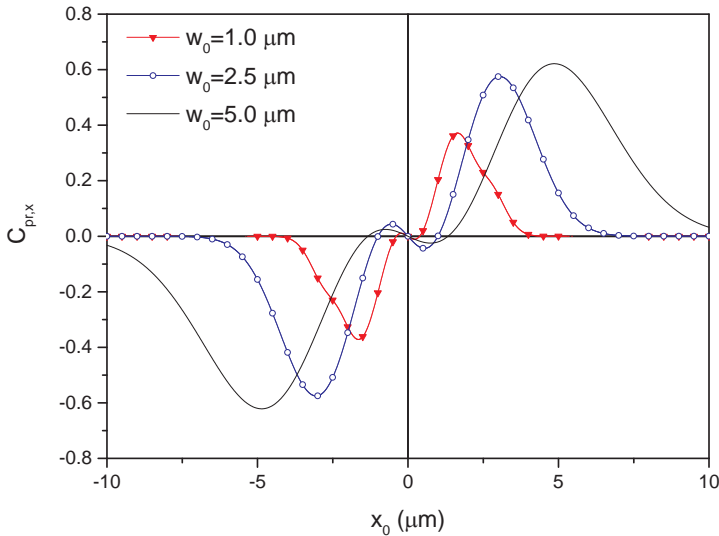

Figure 4. Transverse cross-section $1\mu m$ versus x_0=0 with parameter x_0=0. w_0, w_0, $C_{pr,x}$, x_0, w_0 and λ =0.5μm

To clarify the physical explanation of some features of RPCS, it is necessary for us to consider the contribution of each mode p to RPCS. The contribution of each p mode to RPCS can be computed separately by considering a single term in Eq. (64). Now we consider the contribution of a single p mode to transverse RPCS m_1=1.5. Here we set beam-waist radius m_2=1.

It is shown in Fig. 5 the transverse RPCS y_0=0 versus a=2.5μm with parameter p_{max}=∞. In the calculation, the beam-waist radius is assumed $C_{pr,x}$. Comparison of Fig. 5 with Fig. 4 shows that when w_0=5μm the results obtained by DSE are identical to those by GLMT. In fact, when

$C_{pr,x}$ is large enough, the difference between two theories should be negilible. For example, if x_0, the results of DSE is very close to GLMT results. Special attention should be paid to the case of p_{max}. Fig. 5 shows that when $w_0=5\mu m$, the agreement between the results of GLMT and DSE is already good. This concludes that main contribution of RPF comes from the scattering processes of diffraction ($p_{max} \rightarrow \infty$), specular reflection ($p_{max}$) and direct transmission ($=$ $p_{max}=100$).
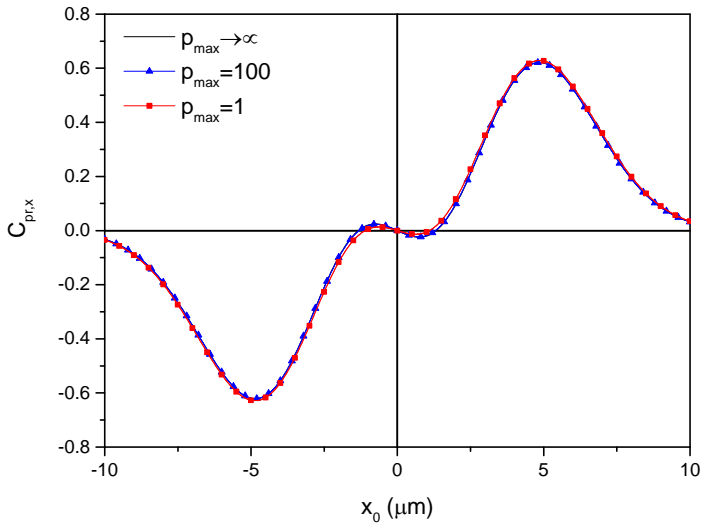

Figure 5. Transverse cross-section $p_{max}=1$ versus $p_{max}=1$ with parameter $p=-1$. $p=0$, $p=1$, $C_{pr,x}$, x_0, p_{max} and $\lambda=0.5\mu m$.

To clarify the physical explanation of some phenomena of RPF, it is necessary to consider the contribution of each mode p to RPCS, which can be computed separately by considering a single term in Eq. (64). Now we consider the contribution of a single p mode to transverse RPCS $m_1=1.5$. Fig.6 depicts the transverse RPCS $m_2=1$ versus $y_0=0$ for $a=2.5\mu m$ and $w_0=5\mu m$. Generally, the RPF at $C_{pr,x}$ is zero for any mode p because of the symmetry. The magnitude of $C_{pr,x}$ for x_0 is much greater than that for $p=1$. This validates that the transverse RPCS $p=2$ is dominated by the contributions of direct transmission ($x_0=0$). Note that the curve for $C_{pr,x}$ has two equilibrium points at about $p=1$, while the curve for $p=2$ has only one points at $C_{pr,x}$. Near the beam axis ($p=1$), the curvesfor $p=2$ has positive slope, while that for $x_0=\pm 1.3\mu m$ has negative one. To explain such phenomena, we must consider the integral effect of all intensity peaks.
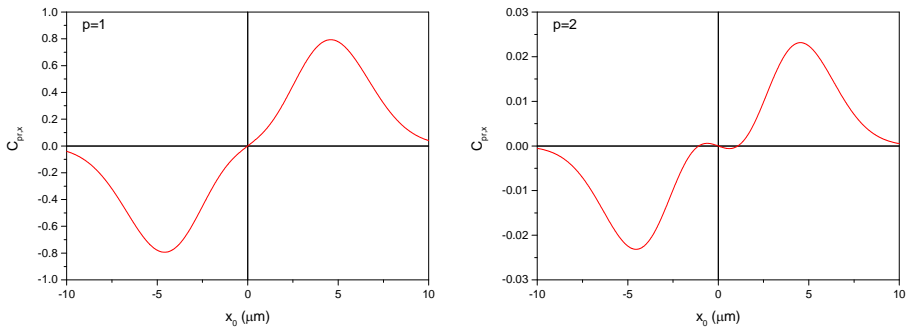
$=$

$=$ μ

Figure 6. Transverse cross-section $p=1$ versus $x_0=0$ corresponding to single mode p. $x_0=0$, $p=1$, $p=2$, $C_{pr,x}$ x_0 and $\lambda=0.5\mu m$.

5. Conclusions

Rigorous theories including GLMT and DSE for RPF exerted on spheres induced by CVB is derived. The incident beam is described by a set of BSCs which is calculated by integral localized approximation, and the scattering coefficients are expanded using Debye series. For very small particles, namely Rayleigh particles, an approximation model is also given. Such thoery can be easily extended to the RPF exerted on multilayered sphere, and also to the RPF induced by other beams. Debye series is used to isolate the contribution of various scattering process to the RPF. The results are of special importance for the improvement of optical tweezers system.

Acknowledgements

Author details

Renxian Li*, Lixin Guo, Bing Wei, Chunying Ding and Zhensen Wu

*Address all correspondence to: rxli@mail.xidian.edu.cn

School of Physics and Optoelectronic Engineering, Xidian University, China

References

[1]   Dholakia,, Dholakia, K.K., Reece, P.. Optical micromanipulation takes hold. Nano To-
      day 2006;1(1):18–27.

[2]   Neuman,, K.C.,, Block, S.. Optical trapping. Rev Sci Instrum 2004;75:2787.

[3]   Enger, J., Goksor, M., Ramser, K., Hagberg, P., Hanstorp, D.. Optical tweezers ap-
      plied to a microfluidic system. Lab Chip 2004;4(3):196–200.

[4]   Domachuk, P., Cronin-Golomb, M., Eggleton, B., Mutzenich, S., Rosengarten, G.,
      Mitchell, A.. Application of optical trapping to beam manipulation in optofluidics.
      Opt Express 2005;13(19):7265–7275.

[5]   Ashkin, A.. Forces of a single-beam gradient laser trap on a dielectric sphere in the
      ray optics regime. Biophys J 1992;61(2):569–582.

[6]   Roosen, G.. A theoretical and experimental study of the stable equilibrium positions
      of spheres levitated by two horizontal laser beams. Opt Commun 1977;21(1):189–194.

[7]   Yao, X., Li, Z., Cheng, B., Zhang, D.. Analysis and calculation of the optical force on a
      double-layer dielectric sphere. Acta Optica Si 2000;10:13051310.

[8]   Chaumet, P.C., Rahmani, A., Nieto-Vesperinas, M.. Optical trapping and manipula-
      tion of nano-objects with an apertureless probe. Phys Rev Lett 2002;88(12):123601.

[9]   Barton, J. P., Alexander, D.R., Schaub, S.A.. Theoretical determination of net radia-
      tion force and torque for a spherical particle illuminated by a focused laser beam. J
      Appl Phys 1989;66(10):4594–4602.

[10] Ren, K.F., Gréhan, G., Gouesbet, G.. Prediction of reverse radiation pressure by gen-
      eralized Lorenz-Mie theory. Appl Opt 1996;35(15):2702–2710.

[11] Ren, K., Gréhan, G., Gouesbet, G.. Radiation pressure forces exerted on a particle ar-
      bitrarily located in a Gaussian beam by using the generalized Lorenz-Mie theory,
      and associated resonance effects. Opt Commun 1994;108(4-6):343–354.

[12] Lock, J.A.. Calculation of the radiation trapping force for laser tweezers by use of
      generalized Lorenz-Mie theory. i. localized model description of an on-axis tightly
      focused laser beam with spherical aberration. Appl Opt 2004;43(12):2532–2544.

[13] Lock, J.A.. Calculation of the radiation trapping force for laser tweezers by use of
      generalized Lorenz-Mie theory. ii. on axis trapping force. Appl Opt 2004;43(12):2545–
      2554.

[14] Gouesbet, G., Maheu, B., Gréhan, G.. Light scattering from a sphere arbitrarily locat-
      ed in a Gaussian beam, using a bromwich formulation. J Opt Soc Am A 1988;5(9):
      1427–1443.

[15] Polaert, H., Gréhan, G., Gouesbet, G.. Forces and torques exerted on a multilayered spherical particle by a focused Gaussian beam. Opt Commun 1998;155(1-3):169–179.

[16] Xu, F., Ren, K.F., Gouesbet, G., Cai, X., Gréhan, G.. Theoretical prediction of radiation pressure force exerted on a spheroid by an arbitrarily shaped beam. Phys Rev E 2007;75(2):026613.

[17] Li, R., Han, X., Shi, L., Ren, K., Jiang, H.. Debye series for Gaussian beam scattering by a multilayered sphere. Appl Opt 2007;46(21):4804–4812.

[18] Li, R., Han, X., Ren, K.F.. Debye series analysis of radiation pressure force exerted on a multilayered sphere. Appl Opt 2010;49(6):955–963.

[19] Bo Sun, Yohai Roichman, and David G. Grier, Theory of holographic optical trapping, Optics Express 2008, 16: 15765-15776

[20] Anna T. O'Neil, Miles J. Padgetta, Axial and lateral trapping efficiency of Laguerre–Gaussian modes in inverted optical tweezers, Optics Communications 2001, 193: 45–50

[21] Garces-Chavez, V., McGloin, D., Melville, H., Sibbett, W., Dholakia, K., et al. Simultaneous micromanipulation in multiple planes using a self-reconstructing light beam. Nature 2002;419(6903):145–147.

[22] Arlt, J., Garces-Chavez, V., Sibbett, W., Dholakia, K.. Optical micromanipulation using a Bessel light beam. Opt Commun 2001;197(4-6):239–245.

[23] Garc´es-Ch´avez, V., Roskey, D., Summers, M., Melville, H., McGloin, D., Wright, E., Dholakia, K.. Optical levitation in a Bessel light beam. Appl Phys Lett 2004;85:4001.

[24] Cizm´ar, T.. Optical traps generated by non-traditional beams. Ph. D. thesis, Masaryk University in Brno; 2006.

[25] Ambrosio, L., Hern´andez-Figueroa, H., et al. Gradient forces on double-negative particles in optical tweezers using Bessel beams in the ray optics regime. Opt Express 2010;18(23):24287– 24292.

[26] Ambrosio, L., Hern´andez-Figueroa, H., et al. Radiation pressure cross sections and optical forces over negative refractive index spherical particles by ordinary Bessel beams. Appl Opt 2011;50(22):4489–4498.

[27] Milne, G., Dholakia, K., McGloin, D., Volke-Sepulveda, K., Zem´anek, P.. Transverse particle dynamics in a Bessel beam. Opt Express 2007;15(21):13972–13987.

[28] Preston, T.C., Mason, B.J., Reid, J.P., Luckhaus, D., Signorell, R.. Size-dependent position of a single aerosol droplet in a Bessel beam trap. Journal of Optics 2014;16(2): 025702.

[29] Q. Zhan, Cylindrical vector beams: from mathematical concepts to applications, Advances in Optics and Photonics 2008, 1:1-57.

[30] Q. Zhan, Trapping metallic Rrayleigh particles with radial polarization, Opt. Express 2004, 12: 3377-3382.

[31] Y. Kozawa and S. Sato, Optical trapping of micrometer-sized dielectric particles by cylindrical vector beams, Opt. Express 2010, 18: 10828-10833.

[32] L. Huang, H. Guo, J. Li, L. Ling, B. Feng, and Z.-Y. Li, Optical trapping of gold nano-particles by cylindrical vector beam, Opt. Lett. 2012, 37:1694-1696.

[33] G. Volpe, D. Petrov, Generation of cylindrical vector beams with few-mode fibers excited by Laguerre–Gaussian beams 2004, Opt. Commun. 237: 89–95.

[34] Ren, K.F., Gouesbet, G., Gr´ehan, G.. Integral localized approximation in generalized lorenz-mie theory. Appl Opt 1998;37(19):4218–4225.